# Self-trapping under the two-dimensional spin-orbit-coupling and spatially growing repulsive nonlinearity

Rongxuan Zhong<sup>1</sup>, Zhaopin Chen<sup>2</sup>, Chunqing Huang<sup>1</sup>, Zhihuan

Luo<sup>3</sup>, Haishu Tan<sup>1</sup>, Boris A. Malomed<sup>2,4,1</sup>, Yongyao Li<sup>1\*</sup>

<sup>1</sup>School of Physics and Optoelectronic Engineering, Foshan University, Foshan 528000, China

<sup>2</sup> Department of Physical Electronics, School of Electrical Engineering,
Faculty of Engineering, Tel Aviv University, Tel Aviv 69978, Israel.

<sup>3</sup>College of Electronic Engineering, South China Agricultural University, Guangzhou 510642, China

<sup>4</sup>ITMO University, St. Petersburg 197101, Russia

We elaborate a method for the creation of two- and one-dimensional (2D and 1D) self-trapped modes in binary spin-orbit (SO)-coupled Bose-Einstein condensates (BECs) with the contact repulsive interaction, whose local strength grows fast enough from the center to periphery. In particular, an exact semi-vortex (SV) solution is found for the anti-Gaussian radial-modulation profile. The exact modes are included in the numerically produced family of SV solitons. Other families, in the form of mixed modes (MMs), as well as excited state of SVs and MMs, are produced too. While the excited states are unstable in all previously studied models, they are partially stable in the present one. In the 1D version of the system, exact solutions for the counterpart of the SVs, namely, semi-dipole solitons, are found too. Families of semi-dipoles, as well as the 1D version of MMs, are produced numerically.

Keywords: Spin-orbit coupling, semi-vortex, mixed mode, excited states.

PACS numbers: 03.75.Lm; 05.45.Yv

### I. INTRODUCTION

For a long time, prediction and experimental creation of stable two- and three dimensional (2D and 3D) solitons remains a challenging problem of nonlinear physics. A commonly known difficulty is that fundamental multidimensional solitary modes in 2D and 3D media with the ubiquitous cubic self-focusing nonlinearity are made unstable, respectively, by the critical and supercritical collapse [1, 2] in the 2D and 3D geometry. Solitons with embedded vorticity (alias vortex rings and tori) [3] are destabilized by a still stronger splitting azimuthal instability. Elaboration of methods for stabilization of multidimensional fundamental and vortex solitons is an issue of great interest to nonlinear photonics and mean-field dynamics in Bose-Einstein condensates (BECs)[4]-[9].

A method which makes it possible to produce exceptionally robust multidimensional modes is based on using the repulsive (defocusing) nonlinearity, whose local strength grows from the center to periphery, in the space of dimension D, at any rate faster than  $R^D$ , as demonstrated in a number of theoretical works [10]-[18]. This type of the nonlinearity modulation can be induced by means of various techniques. In optical media, one may use nonlinearity-enhancing dopants with an inhomogeneous density [19]. In BEC, the tunability of the local nonlinearity by means of the magnetic Feshbach resonance (FR) [20, 21] suggests a possibility for the creation of spatially modulated nonlinearity profiles by means of appropriately shaped magnetic fields [22], which was realized in the experiment [23]. Furthermore, nearly arbitrary spatial profiles of the self-repulsive nonlinearity can be imposed by means of the optically controlled FR [24, 25], as well as with the help of combined magneto-optical shaping [26]. A nonlocal version of this setting may be realized in terms of the long-range interaction between dipolar moments locally induced by a nonuniform dc electric field [27–29].

The other promising method for the stabilization of 2D and 3D solitons relies upon the use of the effective spin-orbit (SO) coupling in binary condensates. The possibility to emulate effects of the SO coupling, originally known in the physics of semiconductors, in two-component atomic BEC has been demonstrated experimentally and analyzed in detail theoretically [30]-[37]. The SO coupling in BEC being a linear interaction between spatially inhomogeneous states in the two components, its interplay with the intrinsic nonlinearity of the BEC makes it possible to predict diverse nonlinear phenomena [38]-[60]. In particular, a noteworthy result, which opens the way to novel applications of the SO coupling in the studies of matter waves, is the stabilization of 2D solitons in the free space, in the form of semi-vortices (SVs) (alias half-vortices [40]), with the vorticity carried by one component of the spinor complex, and

<sup>\*</sup>Electronic address: yongyaoli@gmail.com

mixed-modes (MMs), which combine terms with zero and nonzero vorticities in each component [64–66]. These results break a commonly adopted paradigm stating that bright solitons supported by cubic self-attractive nonlinearities in the free space are always unstable, due to the presence of the critical collapse in the same system [1, 2]. In other words, the stable SVs and MMs play the role of the ground state, which is missing in the 2D free-space settings with the cubic self-attraction, in the absence of the SO coupling [64, 65].

In optics, it has been demonstrated that spatiotemporal solitons in a planar dual-core Kerr-nonlinear waveguide can be stabilized by temporal dispersion of the linear coupling between the cores, which provides for an optical counterpart of the SO coupling [67]. Further, as concerns emulation of the SO coupling in photonics, interest was recently drawn to effects in exciton-polariton condensates in microcavities [68]-[71].

In the 3D setting, it was found that the interplay of the SO coupling with the attractive cubic nonlinearity in the free space creates metastable 3D solitons of the same types as in 2D, viz., SVs and MMs [72]. The SO coupling also helps one to build stable solitons under the action of long-range dipole-dipole interactions in binary BECs. As reported in Refs. [73–75], these may be striped modes and anisotropic vortices, as well as stable 2D gap solitons, supported by the combination of the SO coupling and Zeeman splitting, in the case when the kinetic-energy terms may be neglected in the respective 2D system [60, 61]. Peculiarities of the collapse in the SO-coupled system were explored in Refs. [62] and [63].

The objective of this work is to study solitons in the setting which was not explored before, namely, the SO coupling acting in a combination with self-repulsive contact nonlinearity, which induces self-trapping due to the growth of its local strength from the center to periphery, similar to what was introduced (in the absence of the SO-coupling) in Refs. [10] and [11]. In particular, we find stable analytical solutions for 2D solitons of the SV type, which, to the best of our knowledge, is the first example of solitons available in an exact form under the action of the SO coupling. Stable 2D solitons of the MM type, as well as unstable excited states of SVs and MMs, are found in a numerically form. Exact solitons solutions are also reported for the 1D version of the spinor system.

The paper is structured as follows. The model is introduced in Section II, which is followed by the presentation of the analytical and numerical solutions for SV solitons and results for their stability in Section III. Solitons of the MM type are addressed by means of numerical methods in Section IV. Further, excited states of the SVs and MMs are considered in Section V. Exact analytical solutions and families of numerically found ones in the 1D version of the system are the subject of the consideration in Section VI. The paper is concluded by Section VII.

# II. THE MODEL

In the usual mean-field approximation, the evolution of the spinor wave functions of the spinor BEC,  $\psi = (\psi_+, \psi_-)$ , is governed by the coupled Gross-Pitaevskii equations (GPEs), which include the SO coupling of the Rashba type [76, 77]:

$$i\partial_t \psi_{\pm} = -\frac{1}{2} \nabla^2 \psi_{\pm} + \exp\left(r^2\right) \cdot (|\psi_{\pm}|^2 + \gamma |\psi_{\mp}|^2) \psi_{\pm}$$
$$\pm \lambda (\partial_x \mp i\partial_y) \psi_{\mp} . \tag{1}$$

The equations are written in the scaled form, with  $\lambda$  being the normalized strength of the SO-coupling, and  $\gamma$  the relative strength of the cross-interaction between the two components, with respect to the self-repulsion. Strictly speaking, magnetic field, which imposes the necessary Feshbach-resonance landscape, may differently affect two hyperfine atomic states which compose the SO-coupled system. In the present model, we neglect the difference, to admit analytical solutions. Additional numerical results suggest that, if taken into regard, the difference does not produce conspicuous changes in the results.

In physical units, the SO-coupling strength is characterized by ratio of the respective length scale,  $a_{\rm SO}$ , to the confinement length,  $a_{\perp}$ , which provides for the reduction of the 3D GPEs to the 2D form. In the real experiment, this ratio is usually  $a_{\rm SO}/a_{\perp} \sim 0.1$  [30, 40]. The modulation profile of the repulsive nonlinearity in Eq. (1) is adopted in the anti-Gaussian form, as it makes it possible to find particular exact solutions for the self-trapped states, cf. Ref. [11]. Qualitatively, this steep profile does not lead to results dramatically different from those produced by milder profiles [10, 11].

Stationary states with chemical potential  $\mu$  are looked for as usual,  $\psi_{\pm}(x,y,t) = \phi_{\pm}(x,y)e^{-i\mu t}$ , where  $\phi_{\pm}$  are complex stationary wave functions. These states are characterized by the total norm, proportional to the number of atoms in the binary BECs:

$$N = N_{+} + N_{-} = \int \int (|\psi_{+}|^{2} + |\psi_{-}|^{2}) dx dy.$$
 (2)

Further, the total energy of the soliton is

$$E = E_{\rm K} + E_{\rm N} + E_{\rm SO},\tag{3}$$

where  $E_{\rm K}$  is the kinetic term, while  $E_{\rm N}$  and  $E_{\rm SO}$  are energies of the nonlinear and SO interactions:

$$E_{K} = \frac{1}{2} \int d\mathbf{r} \left( |\nabla \psi_{+}|^{2} + |\nabla \psi_{-}|^{2} \right),$$

$$E_{N} = \frac{1}{2} \int d\mathbf{r} e^{+r^{2}} \left( |\psi_{+}|^{4} + |\psi_{-}|^{4} + 2\gamma |\psi_{+}|^{2} ||\psi_{-}|^{2} \right),$$

$$E_{SO} = \lambda \int d\mathbf{r} \left[ \psi_{+}^{*} \left( \partial_{x} - i\partial_{y} \right) \psi_{-} - \psi_{-}^{*} \left( \partial_{x} + i\partial_{y} \right) \psi_{+} \right].$$
(4)

In the case of the SV solitons,  $\psi_+$  and  $\psi_-$  are defined as the zero-vorticity and vortical components, respectively. Actually, the SVs are the simplest axisymmetric fundamental modes existing in the system. It is relevant to define the relative share of the total norm carried by the vortex component:

$$F_{-} = N_{-}/N. \tag{5}$$

Stability of the solitons was investigated numerically by computing eigenvalues for small perturbations, and the results were subsequently verified by means of direct simulations of Eq. (1). To this end, the perturbed solution was taken as

$$\psi_{\pm} = (\phi_{\pm} + u_{\pm}e^{-i\Lambda t} + v_{\pm}^*e^{i\Lambda^*t})e^{-i\mu t}.$$
 (6)

where \* stands for the complex conjugate. The substitution of this in Eq. (1) and linearization leads to a system of four equations:

$$(\mu + \Lambda)u_{+} = -\frac{1}{2}\nabla^{2}u_{+} + \lambda(\partial_{x} - i\partial_{y})u_{-} + e^{r^{2}}\left(2|\phi_{+}|^{2} + \gamma|\phi_{-}|^{2}\right)u_{+} + e^{r^{2}}\left(\phi_{+}^{2}v_{+} + \gamma\phi_{+}\phi_{-}v_{-} + \gamma\phi_{-}^{*}\phi_{+}u_{-}\right),$$

$$(\mu + \Lambda)u_{-} = -\frac{1}{2}\nabla^{2}u_{-} - \lambda(\partial_{x} + i\partial_{y})u_{+} + e^{r^{2}}\left(2|\phi_{-}|^{2} + \gamma|\phi_{+}|^{2}\right)u_{-} + e^{r^{2}}\left(\phi_{-}^{2}v_{-} + \gamma\phi_{-}\phi_{+}v_{+} + \gamma\phi_{+}^{*}\phi_{-}u_{+}\right),$$

$$(\mu - \Lambda)v_{+} = -\frac{1}{2}\nabla^{2}v_{+} + \lambda(\partial_{x} + i\partial_{y})v_{-} + e^{r^{2}}\left(2|\phi_{+}|^{2} + \gamma|\phi_{-}|^{2}\right)v_{+} + e^{r^{2}}\left(\phi_{+}^{*2}u_{+} + \gamma\phi_{+}^{*}\phi_{-}^{*}u_{-} + \gamma\phi_{-}\phi_{+}^{*}v_{+}\right),$$

$$(\mu - \Lambda)v_{-} = -\frac{1}{2}\nabla^{2}v_{-} - \lambda(\partial_{x} - i\partial_{y})v_{+} + e^{r^{2}}\left(2|\phi_{-}|^{2} + \gamma|\phi_{+}|^{2}\right)v_{-} + e^{r^{2}}\left(\phi_{-}^{*2}u_{-} + \gamma\phi_{-}^{*}\phi_{+}^{*}u_{+} + \gamma\phi_{+}\phi_{-}^{*}v_{+}\right).$$

$$(7)$$

This system leads to the eigenvalue problem for the perturbation eigenfrequency,  $\Lambda = \Lambda_r + i\Lambda_i$ , written in the matrix form:

$$\begin{pmatrix} A_{11} & A_{12} & A_{13} & A_{14} \\ A_{21} & A_{22} & A_{23} & A_{24} \\ A_{31} & A_{32} & A_{33} & A_{34} \\ A_{41} & A_{42} & A_{43} & A_{44} \end{pmatrix} \begin{pmatrix} u_{+} \\ u_{-} \\ v_{+} \\ v_{-} \end{pmatrix} = \Lambda \begin{pmatrix} u_{+} \\ u_{-} \\ v_{+} \\ v_{-} \end{pmatrix},$$
(8)

with matrix elements defined as

$$A_{11} = -\frac{1}{2}\nabla^{2} - \mu + e^{r^{2}} \left( 2|\phi_{+}|^{2} + \gamma|\phi_{-}|^{2} \right),$$

$$A_{12} = \lambda(\partial_{x} - i\partial_{y}) + e^{r^{2}} \gamma \phi_{+}^{*} \phi_{+},$$

$$A_{13} = e^{+r^{2}} \phi_{+}^{2}, \quad A_{14} = e^{+r^{2}} \gamma \phi_{+} \phi_{-};$$

$$A_{21} = -\lambda(\partial_{x} + i\partial_{y}) + e^{r^{2}} \gamma \phi_{+}^{*} \phi_{-},$$

$$A_{22} = -\frac{1}{2}\nabla^{2} - \mu + e^{r^{2}} \left( 2|\phi_{-}|^{2} + \gamma|\phi_{+}|^{2} \right)$$

$$A_{23} = A_{14}, \quad A_{24} = e^{r^{2}} \phi_{-}^{2},$$

$$A_{31} = -A_{13}^{*}, \quad A_{32} = -A_{23}^{*},$$

$$A_{33} = -A_{11}^{*}, \quad A_{34} = -A_{12}^{*}$$

$$A_{41} = -A_{14}^{*}, \quad A_{42} = -A_{24}^{*},$$

$$A_{43} = -A_{21}^{*}, \quad A_{44} = -A_{22}^{*}.$$

$$(9)$$

The unperturbed solution  $\phi_{\pm}$  is stable if all the eigenvalues  $\Lambda$  are real.

# III. SEMI-VORTEX (SV) SOLITONS

#### A. The exact solution

We adopt an ansatz for SV solutions to Eq. (1), with chemical potential  $\mu$ , as

$$\psi_{+}(x, y, t) = e^{-i\mu t} f_{1}(r^{2}) 
\psi_{-}(x, y, t) = e^{-i\mu t + i\theta} r f_{2}(r^{2}).$$
(10)

where  $(r, \theta)$  are the polar coordinates, and real functions  $f_{1,2}(r^2)$  obey the following equations:

$$\mu f_{1} + 2 \left(r^{2} f_{1}^{"} + f_{1}^{'}\right) - \exp\left(r^{2}\right) \cdot \left(f_{1}^{2} + \gamma r^{2} f_{2}^{2}\right) f_{1}$$

$$-2\lambda \left(r^{2} f_{2}^{'} + f_{2}\right) = 0$$

$$\mu f_{2} + 2 \left(r^{2} f_{2}^{"} + 2 f_{2}^{'}\right) - \exp\left(r^{2}\right) \cdot \left(r^{2} f_{2}^{2} + \gamma f_{1}^{2}\right) f_{2}$$

$$+2\lambda f_{1}^{'} = 0,$$
(11)

where

$$f_{1,2}' \equiv \frac{d}{d(r^2)} f_{1,2} \quad f_{1,2}'' \equiv \frac{d^2}{d(r^2)^2} f_{1,2}.$$
 (12)

Further, assuming

$$f_{1,2} = A_{\pm} \exp\left(-r^2/2\right),$$
 (13)

and substituting this in Eq. (11), it is easy to see that Eqs. (10) and (13) indeed produce an exact solution, provided that the constants are expressed in terms of  $\gamma$  as follows:

$$\lambda^2 = \frac{(1-\gamma)(2-\gamma)}{4},\tag{14}$$

$$\mu = \frac{(2-\gamma)}{2(1-\gamma)} + \gamma,\tag{15}$$

$$A_{+} = \left[\frac{2 - \gamma}{2(1 - \gamma)}\right]^{1/2}.\tag{16}$$

$$A_{-}^{2} = 1/2. (17)$$

In particular, Eq. (14) implies that the present exact solution is a particular one (rather than being generic), because it exists only if the SO-coupling strength is adjusted to the value fixed by Eq. (14). With regard to these results, the norm of each component of the soliton is

$$N_{+} = \frac{\pi(2-\gamma)}{2(1-\gamma)},\tag{18}$$

$$N_{-} = \frac{\pi}{2},\tag{19}$$

$$N = N_{+} + N_{-} = \frac{\pi}{2} \left( \frac{2 - \gamma}{1 - \gamma} + 1 \right), \tag{20}$$

and the share of the total norm in the vortical component [see Eq. (5)] is

$$F_{-} = \frac{1 - \gamma}{3 - 2\gamma}.\tag{21}$$

Equations (14)-(20) suggest that the exact solution is solely controlled by  $\gamma$ , and moreover, Eq. (14) demonstrates that the exact solution does not exists for  $1 \le \gamma \le 2$ . According to Eqs. (18) and (19), for  $0 \le \gamma < 1$  (the cross-repulsion is weaker than the self-repulsion), one has  $N_+ > N_-$  (the fundamental component is the larger one); however, for  $\gamma > 2$ , the situation is opposite, featuring a larger vortex component:  $N_+ < N_-$ .

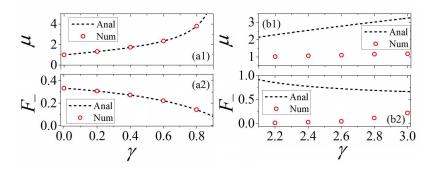


FIG. 1: (a1,a2) Comparison between the analytical and numerical results (the black dashed curve and red circles, respectively) for the soliton's chemical potential,  $\mu$ , and the norm share in the vortical component,  $F_-$ , in the region of  $0 \le \gamma < 1$ . (b1,b2) The same for  $\gamma > 2$ . Parameters  $\lambda$  (the strength of the SO coupling) and N (the total norm) are here taken as per by Eqs. (14) and (20), respectively. The dashed curves for  $\mu(\gamma)$  and  $F_-(\gamma)$  are plotted, severally, as per Eqs. (15) and (21).

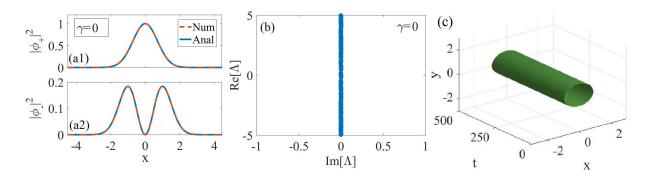


FIG. 2: (a1,a2) The comparison between the analytical and numerically found (blue solid and red dashed curves) stationary profiles of the soliton's wave function, shown in cross-section y=0, at  $\gamma=0$ . (b) Spectra of stability eigenvalues  $\Lambda$  for the exact solution from panels (a1,a2). (c) Direct simulations of the evolution of this soliton (with 2% random noise added to the initial conditions), shown by the contour plot of the density profile,  $|\psi_{+}(\mathbf{r},t)|^2$ . In this figure, the analytical wave function is taken as per Eqs. (10), (13), (16) and (17), while  $\lambda$  and N are given by Eqs. (14) and (20).

For comparison with the analytical results, we used numerically found solutions for the ground state of the present system, which were generated, for the same values of parameters, by means of the imaginary-time method. The comparison for the soliton's chemical potential and the norm share of the vortical component,  $F_{-}$  [see Eq. (5)], in

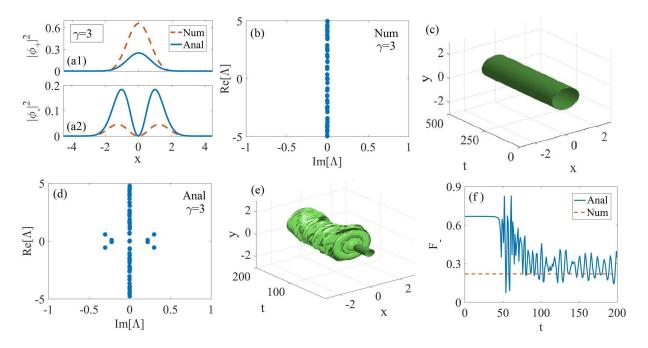


FIG. 3: (a1,a2) Comparison between the analytical solution and numerically found ground state results (the blue solid and red dashed curves, respectively), shown in cross-section y=0, at  $\gamma=3$ . (b) Spectra of the stability eigenvalues,  $\Lambda$ , for the numerical solution (the one represented by the red dashed curves in panels (a1,a2). (c) Direct simulations to the evolution of the numerical solution (with 2% random noise added to the initial conditions), shown by the contour plot of the density profile,  $|\psi_+(\mathbf{r},t)|^2$ . (d) Spectra of the stability eigenvalues  $\Lambda$  for the analytical solution (represented by the blue solid curve in panels (a1,a2). (e) Direct simulations of the perturbed evolution of the analytical solution, shown by the contour plot of the density profile,  $|\psi_+(\mathbf{r},t)|^2$ . (f)  $F_-$ , defined as per Eq. (5), as observed in the direct simulations initiated by the exact solution and the numerical one (the blue solid and red dashed curves, respectively). The analytical solution dealt with in this figure is taken as per Eqs. (10), (13), (16) and (17), while parameters  $\lambda$  and N are defined by Eqs. (14) and (20).

the regions of  $0 \le \gamma < 1$  and  $\gamma > 2$  is displayed in Fig. 1. Figures 1(a1,a2) show that the analytical solution exactly produces the ground state for  $0 \le \gamma < 1$ . The comparison of the respective wave-function profiles, as produced by the numerical and exact solutions in this case, is presented in Figs. 2(a1,a2). Further, Figs. 2(b) and (c) corroborate the stability of the exact solution, which should be expected from the ground state.

However, in the region of  $\gamma > 2$ , Figs. 1(b1,b2) and 3(a1,a2) show that the analytical solution is different from the ground states. In particular, Fig. 1(b2) shows that the numerically found ground state always has  $F_- < 0.5$  (i.e., the zero-vorticity components remains the dominant one), while the exact solution has  $F_- > 0.5$  at  $\gamma \ge 2$ . Thus, the exact solution represents an excited state of the SV, which is unstable, as seen in Figs. 3(d-f), on the contrary to the stability of the numerically found ground state, corroborated by Figs. 3(b,c). Lastly, the evolution of the norm share in the vortical component,  $F_-(t)$ , displayed in Fig. 3(f), suggests that the evolution of the unstable exact SV at  $\gamma > 2$  tends to transform it towards the stable ground state. We note that full soliton family in the system depends not only on  $\gamma$ , but also on other control parameters, viz, N and  $\lambda$ . Thus, the exact solution produces only specific subfamilies of the solitons, possible links between which are not available in the analytical form. In the following subsection, we produce numerical results for a broader soliton family, into which the analytical branches may be embedded.

#### B. Full numerical results

In the numerical form, soliton solutions were obtained by means of the imaginary-time method. To this end, the same input was used as in Ref. [64], which agrees with the general SV ansatz (10):

$$\phi_{+}^{(0)}(r,\theta) = A_{+} \exp(-\alpha_{+}r^{2}), \ \phi_{-}^{(0)}(r,\theta) = A_{-}r \exp(i\theta - \alpha_{-}r^{2}), \tag{22}$$

with real constants  $A_{\pm}$  and  $\alpha_{\pm}$ . The control parameters are N,  $\gamma$ , and  $\lambda$ .

Figure 4(a) displays the chemical potential of the SV family versus N for different values of  $\gamma$ . The  $\mu(N)$  curves feature a positive slope, with  $d\mu/dN > 0$ , i.e., they satisfy the anti-Vakhitov-Kolokolov criterion, which is conjectured

to provide a necessary stability condition for bright solitons in self-repulsive nonlinear media [78]. SVs with larger values of  $\gamma$  have larger  $\mu$ , which also is a natural corollary of the repulsive sign of the nonlinearity. The negative slope,  $d\mu/d\lambda < 0$ , in Fig. 4(b), for different values of  $\gamma$ , implies that the SO-coupling energy is negative, partly compensating the repulsive nonlinear interactions. The decay of  $F_-(N)$  with the increase of N, observed in Fig. 4(c), shows the same trend as reported for stable SVs in the self-attractive system [64], i.e., concentration of the norm in the zero-vorticity component. Note that the  $F_-(N)$  curves of  $F_-(N)$  with different values of  $\gamma$  are degenerate at small N, splitting with the increase of N, the vortical-component's share,  $F_-$ , decaying faster under the action of stronger cross-repulsion (for larger  $\gamma$ ). On the other hand, Fig. 4(d) demonstrates the growth of  $F_-$  with the increase of  $\lambda$ , which is natural too, as stronger SO coupling generates more vorticity, i.e., it causes transfer of the norm to the vortical component. In particular,  $F_-$  becomes nearly independent of  $\gamma$  at  $\lambda > 1$ , which means that the SO interaction between the components dominates over the nonlinear repulsion between them in this case. In Fig. 4, the exact analytical solutions, included in the families of numerically generated ones, are marked by back solid squares.

Lastly, we stress that the SV family, produced by the imaginary-time integration, is found to be completely stable (in terms of stability eigenvalues and direct simulations alike) at all values of the parameters, including all values of  $\gamma$ . The latter conclusion is essential, because, in the 2D SO-coupled system with attractive interactions, the SVs are stable only at  $\gamma \leq 1$  [64].

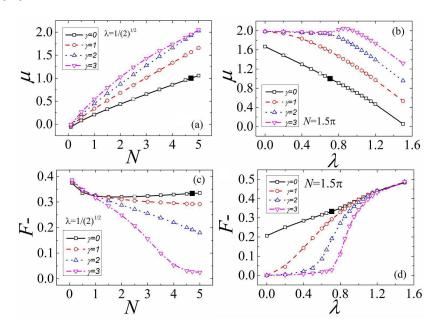


FIG. 4: (a,b) The chemical potential of the numerically found family of semi-vortices,  $\mu$ , versus the total norm, N, and the SO-coupling strength,  $\lambda$ , for different values of the cross/self interaction ratio,  $\gamma=0,\ 1,\ 2,\ 3$ , respectively. (c,d) The norm share in the vortical component,  $F_-$  [see Eq. (5)], versus N and  $\lambda$  for  $\gamma=0,\ 1,\ 2,\$ and 3, respectively. In panels (a,c) and (b,d),  $\lambda=1/\sqrt{2}$  and  $N=1.5\pi$  is fixed, severally. The black solid squares in the panels represent the exact solution, given by Eqs. (10) and (14)-(21), with  $\gamma=0$ .

## IV. FUNDAMENTAL MIXED-MODE (MM) SOLITONS

Following Ref. [64], MM states can be initiated by the input which includes terms with vorticities (0, -1) and (0, +1) in the two components,

$$\phi_{\pm}^{(0)}(r,\theta) = A_1 \exp(-\alpha_1 r^2) \mp A_2 r \exp(-\alpha_2 r^2 \mp i\theta), \tag{23}$$

where  $A_{1,2}$  and  $\alpha_{1,2}$  are real constants, cf. Eq. (22). The initial approximation for the MM states are built as equal-weight superpositions of SVs with topological content (0, -1) and (0, +1) in the two components. In a certain sense, the SVs and MMs are similar, respectively, to immiscible and miscible states in binary superfluids. Unlike the SVs, MMs cannot be represented by an exact ansatz, but numerical and variational results clearly confirm their existence. A typical example of a stable MM with  $(N, \gamma, \lambda) = (2, 0, 1)$ , generated by the imaginary-time integration, is shown in Fig. 5.

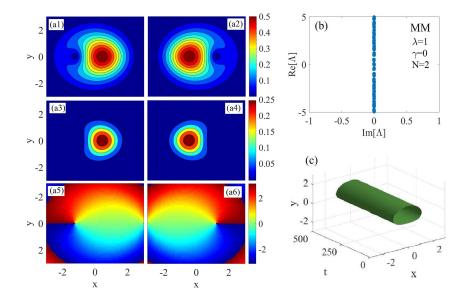


FIG. 5: (a) A typical example of a stable MM (mixed-mode) soliton, shown by  $|\phi_{\pm}(\mathbf{r})|$  (a1,a2),  $|\phi_{\pm}(\mathbf{r})|^2$  (a3,a4) as well as their phase diagrams (a5,a6), respectively, with  $(N, \gamma, \lambda) = (2, 0, 1)$ . (b) The spectrum of stability eigenvalues for this state. (d) Direct simulation of its evolution with 2% noise, shown by means of the density plot,  $|\phi_{\pm}(\mathbf{r}, t)|^2$ .

The numerical analysis demonstrates that, similar to what is reported above for the SVs, the family of the MM states generated by the imaginary-time simulations from input (23) is completely stable at all values of parameters, including, in particular, all values of  $\gamma$ . This conclusion is essential because, in the 2D SO-coupled system with attractive interactions, MM states are stable solely at  $\gamma \geq 1$  [64], i.e., the MMs are stable, in the care of the attractive nonlinearity, where the SVs are not, and vice versa, coexisting as stable states solely in the case of the Manakov's nonlinearity [79], i.e., at  $\gamma = 1$ . The stability switch between the SVs and MMs was explained in Ref. [64] by the fact that, for equal values of N, the SV has a smaller energy, i.e., it realizes the system's ground state, at  $\gamma < 1$ , while at  $\gamma > 1$  the MM provides for the smaller energy, i.e., the ground state. The SV and MM states are degenerate, having equal energies, at  $\gamma = 1$ , when both are stable.

In the present system, as said above, both the SVs and MMs are completely stable at all values of  $\gamma$ . This conclusion is natural because the system with repulsive interactions has a definite trend to be more stable than its attractive counterpart. Nevertheless, it makes sense to identify the ground state of the present system too, comparing values of energy of the coexisting SV and MM solitons with equal values of the norm. The comparison is shown in Fig. 6(a), which clearly demonstrates that the SV and MM realize the system's ground state at  $\gamma > 1$  and  $\gamma < 1$ , respectively, which is precisely opposite to the situation in the 2D SO-coupled system with the attractive interactions [64]. The same conclusion was obtained for all other values of parameters, i.e., fixed N and  $\lambda$ .

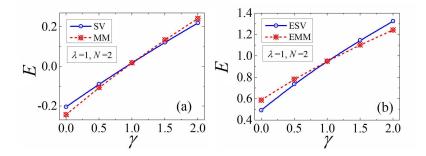


FIG. 6: (a) The total energy of the SV (semi-vortex) and MM (mixed-mode) states (blue solid and dashed red curves, respectively) versus  $\gamma$  for a fixed norm, N=2, and a fixed strength of the SO-coupling,  $\lambda=1$ . (b) The Energy of ESV (excited-state of SV) with  $S_+=1$  and EMM (Excited state of MM) with  $S_1=1$  versus  $\gamma$  for fixed N=2 and  $\lambda=1$ .

#### V. EXCITED STATES

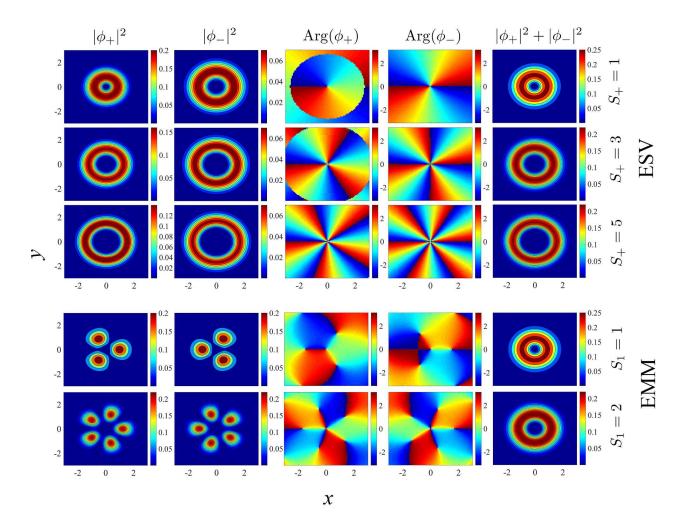


FIG. 7: Examples of stable excited states of SVs ("ESVs") with  $S_+=1$ , 3, and 5 (the first, second, and third rows, respectively), and of MMs ("EMMs") with  $S_1=1$  and 2 (the fourth and fifth rows, respectively). The first and second columns display density patterns of components  $\phi_{\pm}$ , while the third and fourth columns display phase structures of  $\phi_{\pm}$ . The fifth column is the total-density pattern,  $n(\mathbf{r}) = |\phi_+|^2 + |\phi_-|^2$ . Parameters are N=2,  $\gamma=1$  and  $\lambda=1$  for all the panels.

Excited states of SVs and MMs are produced by adding extra vorticity to both components of these states. In particular, as suggested by Ref. [64], excited states of the SVs correspond to the following ansatz compatible with Eq. (1), cf. Eq. (10):

$$\psi_{+}(x,y,t) = e^{-i\mu t + in\theta} r^{n} f_{1}(r^{2})$$

$$\psi_{-}(x,y,t) = e^{-i\mu t + i(n+1)\theta} r^{n+1} f_{2}(r^{2}),$$
(24)

with n=1,2,.... However, in the previously studied systems, all the excited states, unlike the fundamental MMs and SVs, were found to be completely unstable in SO-coupled systems with homogeneous contact nonlinearities [64, 80]. Very recently, stable excited states of SVs and MMs were predicted in the model of the 2D dipolar BEC with long-range interactions between field-induced dipoles whose magnitude grows from the center to periphery [81]. The latter finding suggests to explore the existence and stability of excited in the present system with the contact repulsive interactions.

We have performed the analysis, running imaginary-time simulations initiated by the following inputs for the excited states of SVs:

$$\phi_{\pm}^{(0)} = A_{\pm} r^{|S_{\pm}|} \exp(-\alpha_{\pm} r^2 + iS_{\pm}\theta), \tag{25}$$

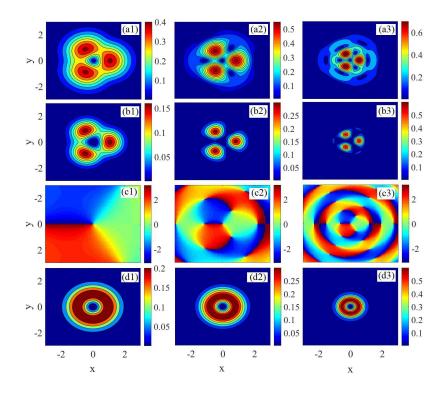


FIG. 8: (a1-a3) $|\phi_{+}|$  with  $\lambda = 0.2$  (a1), 2 (a2) and 4 (a3). (b1-b3)  $|\phi_{+}|^2$  with  $\lambda = 0.2$  (b1), 2 (b2) and 4 (b3). (c1-c3)The phase diagram of  $\phi_{+}$  with  $\lambda = 0.2$  (c1), 2 (c2) and 4 (c3). (d1-d3) Total density pattern  $n(\mathbf{r}) = |\phi_{+}(\mathbf{r})|^2 + |\phi_{-}(\mathbf{r})|^2$  with  $\lambda = 0.2$  (d1), 2 (d2) and 4 (d3). Total norm and  $\gamma$  of these examples are fixed by  $(N, \gamma) = (2, 1)$ . Solitons in these panels are all stable.

cf. the general exact ansatz (24), and for the excited states of MMs:

$$\phi_{\pm}^{(0)} = A_1 r^{|S_1|} \exp(-\alpha_1 r^2 \pm i S_1 \theta) \mp A_2 r^{|S_2|} \exp(-\alpha_2 r^2 \mp i S_2 \theta),$$
(26)

where  $A_{\pm}$ ,  $A_{1,2}$ ,  $\alpha_{\pm}$  and  $\alpha_{1,2}$  are real constants,  $S_{+,1}=0,\pm 1,\pm 2,\cdots$  are integers, and  $S_{-,2}=S_{+,1}+1$ . In Eq. (25), fundamental SVs are produced by  $(S_+,S_-)=(-1,0)$  or (0,1), cf. Eq. (22), and their excited states correspond to  $(S_+,S_-)=(n,n+1)$ , with  $n\neq -1$  or 0. Similarly, Eq. (26) produces fundamental MMs for  $S_1=-1$  and 0, and their excited states correspond to other integer values of  $S_1$ . Below, we fix  $\lambda=1$  and consider  $S_{+,1}\geq 1$ , for  $N\leq 5$  and  $\gamma\leq 2$ .

Numerical results demonstrate that embedded states of SVs may be stable up to  $S_+=5$ , while MMs in the excited states are stable only up to  $S_1=2$ . Examples of the 2D excited states are displayed in Fig. 7. In the case of the SVs, they feature a standard ring structure in each components (see top three rows in Fig. 7), with the topological charges identical to the values of  $S_{\pm}$  in input (25). In the case of MMs, each component of the excited state is built as annular necklace structures, the number of fragments in the necklaces being exactly equal to  $S_1 + S_2 = 2S_1 + 1$ , see two bottom rows in Fig. 7. The total angular momentum of the MM states is  $L = (L_+ + L_-)/2 \equiv 0$ . The total density patterns, i.e.  $|\phi_+(\mathbf{r})|^2 + |\phi_-(\mathbf{r})|^2$ , of the excited states of both SVs and MMs exhibit perfect ring patterns. The dependence of the necklace pattern of the excited MM states on the SO strength,  $\lambda$ , is illustrated by Fig. 8, which displays excited MMs with  $(N, \gamma) = (2, 1)$  and different values of  $\lambda$ . The figure shows that the main density pattern of the excited MM states shrinks with the increase of  $\lambda$ , and higher-order lobes emerge from pattern's core. Recently, somewhat similar 2D necklace patterns were realized by the SO-coupled BEC in an annular trapping potential [82], where they are ground states, featuring a dependence on  $\lambda$  different from that produced by the excited MM states in the current work.

Typical example of the evolution of stable and unstable excited states are displayed in Fig. 9. As mentioned above, excited states of SVs are stable for  $S_+ \leq 5$ . At  $S_+ > 5$ , the instability perturbs the SV pattern, but does not destroy its vortex structure. Excited states of MMs are stable only for  $S_1 = 1$  and 2. Unstable MM excited states tend to transform into fundamental MMs.

The different instability evolution of the SV and MM excited states is explained by the presence of the angular momentum in SVs. As a result, unstable excited states of SVs keep its initial value, which prevents their transformation

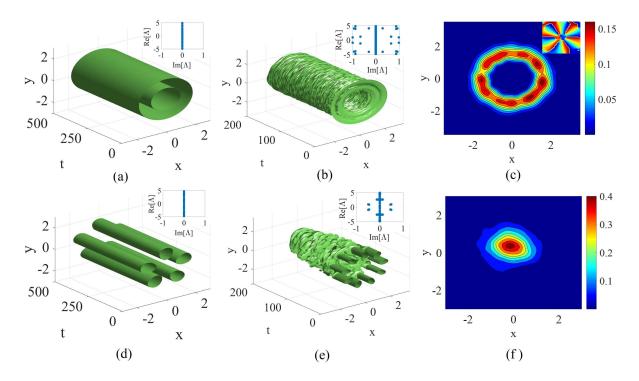


FIG. 9: Example of the real-time evolution of stable and unstable excited states of SVs and MMs. (a) A stable SV's excited state with  $(N, \gamma, \lambda, S_+) = (2, 1, 1, 4)$ . (b) An unstable SV state with  $(N, \gamma, \lambda, S_+) = (2, 1, 1, 6)$ . (c) The final density pattern of  $|\psi_+|^2$ , corresponding to panel (b), the inset showing the respective phase pattern. (d) A stable excited state of the MM with  $(N, \gamma, \lambda, S_1) = (2, 1, 1, 2)$ . (e) An unstable MM state with  $(N, \gamma, \lambda, S_1) = (2, 1, 1, 4)$ . (f) The final density pattern of  $|\psi_+|^2$ , corresponding to panel (e). Spectra of stability eigenvalues for these modes are shown as insets in panels (a), (b), (d) and (e).

into their stable counterparts with smaller values of the angular momentum [see an example in Figs. 9(b,c), where the output phase pattern demonstrate that the vorticity of  $\psi_{+}$  remains 6]. On the other hand, the zero total angular momentum of unstable MM excited states allows them to simplify themselves into the fundamental MM, see an example in Fig. 9(e,f).

Finally, families of the excited states of SVs and MMs are characterized by the corresponding  $E(\gamma)$  dependence, which is displayed in Fig. 6(b) with fixed values of  $S_+$  and  $S_1$  for N=2. This panel shows that the first excited states of SVs and MMs are degenerate, having equal energies, at  $\gamma=1$ . The SV excited states have a lower energy than their counterparts of the MM type at  $\gamma<1$ , and vice versa at  $\gamma>1$ .

### VI. SOLITON IN THE 1D MODEL

The 1D reduction of the 2D system (1) amounts to the following system of coupled GPEs:

$$i\partial_t \psi_{\pm} = -\frac{1}{2} \partial_{xx}^2 \psi_{\pm} + \exp(+x^2) \cdot (|\psi_{\pm}|^2 + \gamma |\psi_{\mp}|^2) \psi_{\pm} \pm \lambda \partial_x \psi_{\mp} .$$
 (27)

Stationary solutions with chemical potential are looked for in the usual form,  $\psi_{\pm}(x,t) = e^{-i\mu t}u_{\pm}(x)$ , where real functions  $u_{\pm}(x)$  (unlike complex stationary wave function in the 2D case) solve equations

$$\mu u_{+} + \frac{1}{2}u_{+}^{"} - e^{x^{2}}(u_{+}^{2} + \gamma u_{-}^{2})u_{+} - \lambda u_{-}^{'} = 0,$$
(28)

$$\mu u_{-} + \frac{1}{2}u_{-}^{"} - e^{x^{2}}(u_{-}^{2} + \gamma u_{+}^{2})u_{-} + \lambda u_{+}^{'} = 0,$$
(29)

where the prime stands for d/dx. A particular exact solution to Eqs. (28) and (29) with one even and one odd components, which may be considered as a 1D counterpart of the 2D SV states, is looked for in the form of

$$u_{+} = A_{+} \exp(-x^{2}/2), \ u_{-} = A_{-}x \exp(-x^{2}/2).$$
 (30)

Equation (30) implies that component  $u_{-}$  has a dipole structure, therefore, modes of this type may be named semidipole solitons. Substituting this in Eqs. (28) and (29), we obtain the following relations between the constants:

$$\mu A_{+} - \frac{1}{2}A_{+} - A_{+}^{3} - \lambda A_{-} = 0,$$

$$\frac{A_{+}}{2} - \gamma A_{-}^{2}A_{+} + \lambda A_{-} = 0,$$

$$\mu A_{-} - \frac{3}{2}A_{-} - \gamma A_{+}^{2}A_{-} - \lambda A_{+} = 0,$$

$$\frac{1}{2}A_{-} - A_{-}^{3} = 0.$$
(31)

Solving Eq. (31), one may obtain

$$\lambda^2 = \frac{(\gamma - 1)(\gamma - 3)}{8},\tag{32}$$

$$\mu = \frac{(\gamma + 1)(2\gamma - 3)}{4(\gamma - 1)},\tag{33}$$

$$A_{+}^{2} = \frac{(\gamma - 3)}{4(\gamma - 1)},\tag{34}$$

$$A_{-}^{2} = \frac{1}{2}. (35)$$

Equation (32) indicates that the exact solution exist in the cases of  $\gamma < 1$  and  $\gamma > 3$ . The norms of the two components of the exact soliton are

$$N_{+} = \frac{\sqrt{\pi}}{4} \left( \frac{\gamma - 3}{\gamma - 1} \right),\tag{36}$$

$$N_{-} = \frac{\sqrt{\pi}}{4}.\tag{37}$$

$$N = N_{+} + N_{-} = \frac{\sqrt{\pi}}{2} \left( \frac{\gamma - 2}{\gamma - 1} \right). \tag{38}$$

Therefore, the 1D version of the analytical result for the relative share of the total norm which is kept in the odd component is

$$F_{-} = \frac{\gamma - 1}{2(\gamma - 2)},\tag{39}$$

cf. Eq. (5). Similar to the exact 2D solution, parameters of the 1D solution,  $\lambda$  and N, are solely defined by  $\gamma$  [cf. Eq. (14) and (20)]. Moreover, according to Eqs. (39), if  $0 \le \gamma < 1$ , then  $F_- < 0.5$  (the fundamental component is the larger one); however, if  $\gamma > 3$ , then  $F_- > 0.5$  (the vortex component is larger).

Comparison between the analytical solution and numerical results, produced by the imaginary-time integration of Eq. (27), for  $\mu$  and  $F_-$  in the regions of  $0 \le \gamma < 1$  and  $\gamma > 3$  is displayed in Fig. 10. Similar to the situation in the 2D system, cf. Fig. 1, in the region of  $0 \le \gamma < 1$  the analytical solution exactly produces the ground state, while at  $\gamma > 3$ , the analytical solution corresponds to some excited state, the ground state being strongly different. The corresponding comparison of the wave functions, as produced by the numerical and exact solutions in the regions of  $0 \le \gamma < 1$  and  $\gamma > 3$ , are displayed in Figs. 11(a1,a2) and 12(a1,a2), respectively.

The stability of the analytical and numerical solutions was verified by numerical computation of the respective eigenvalues and through direct simulations of Eq. (27). Also similar to the 2D case, the simulations show that the analytical exact solution, along with its numerical counterpart, are completely stable in the interval of  $0 \le \gamma < 1$ , see a typical example for  $\gamma = 0.5$  in Fig. 11. On the other hand, in the region of  $\gamma > 3$ , the numerical solution is stable, while the exact one is not. Typical examples of the stable and unstable evolution for  $\gamma = 3.5$  are displayed in Fig. 12.

Following the patterns of the analysis presented in subsection B of Section III, families of generic semi-dipole states can be found by means of the imaginary-time method, applied to Eq. (27) with the input taken as per Eq. (30). Similar to Fig. 4, we characterize the semi-dipole families by plotting  $\mu$  and  $F_{-}$  versus N and  $\lambda$  in the Fig. 13. The exact analytical solution, given by Eqs. (30) and (32)-(39), is included in the figures.

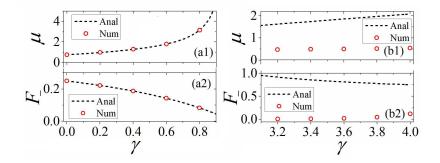


FIG. 10: (a1,a2) The comparison between the exact analytical result (the black dashed curve) and numerical findings, produced by the imaginary-time simulations of the 1D system (red circles) for  $\mu$  and  $F_-$  in the region of  $0 \le \gamma < 1$ . (b1,b2) The same at  $\gamma > 3$ . Parameters  $\lambda$  (the strength of the SO coupling) and N (the total norm) are defined by Eqs. (32) and (38), respectively. The analytical expressions for  $\mu(\gamma)$  and  $F_-(\gamma)$  are given by Eqs. (33) and (39), respectively.

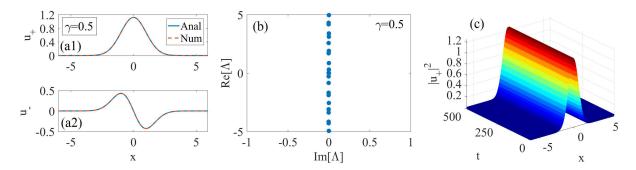


FIG. 11: (a1,a2) The comparison between the analytical and numerical results (the blue solid and red dashed curves) for the 1D wave function with  $\gamma = 0.5$ . (b) The spectrum of stability eigenvalues  $\Lambda$  for the exact solution from panels (a1,a2). (c) Direct simulations of the evolution of this soliton. Here the analytical wave functions are given by Eqs. (10), (30), (34) and (35), while  $\lambda$  and N are defined by Eqs. (32) and (38), respectively.

Further, the 1D version of MMs can also be found in the numerical form, starting from ansatz

$$u_{\pm} = (A_1 \pm A_2 x) \exp(-x^2/2).$$
 (40)

A typical example of the stable 1D MM for  $\gamma = 0$  is displayed in Fig. 14. The  $E(\gamma)$  curves for the 1D semi-dipoles and MMs are shown in the Fig. 14(c), demonstrate that these two species of 1D solitons are almost degenerate, in terms of the energy.

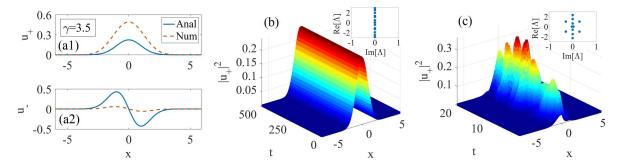


FIG. 12: (a1,a2) Comparison between the analytical and numerically found (the blue solid and red dashed curves, respectively) for the 1D soliton wave function at  $\gamma = 3.5$ . (b,c) Direct simulations to the evolution initiated by the numerical and analytical solution, respectively. Insets are spectra of stability eigenvalues  $\Lambda$  for them. Here the analytical wave functions are defined by Eqs. (10), (30), (34) and (35), while  $\lambda$  and N are defined by Eqs. (32) and (38), respectively.

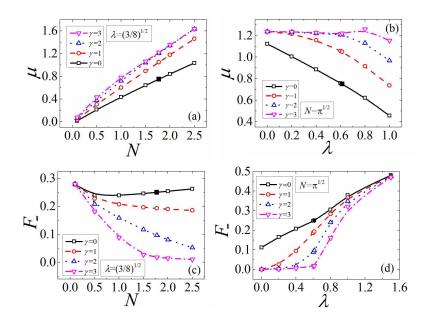


FIG. 13: The chemical potential of the numerically found family of 1D semi-vortices,  $\mu$ , versus the total norm, N, and the SO-coupling strength,  $\lambda$ , for different values of the cross/self interaction ratio,  $\gamma=0, 1, 2, 3$ , respectively. (c,d) The norm share in the vortical component,  $F_-$  [see Eq. (5)], versus N and  $\lambda$  for  $\gamma=0, 1, 2,$  and 3, respectively. In panels (a,c) and (b,d),  $\lambda=\sqrt(3/8)$  and  $N=\sqrt(pi)$  is fixed, severally. The black solid squares in the panels represent the exact solution, given by Eqs. (30)-(39), with  $\gamma=0$ .

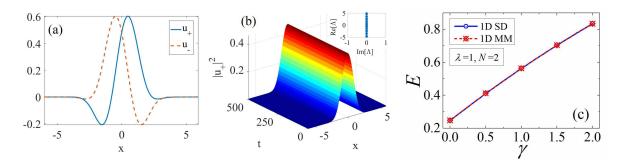


FIG. 14: (a,b)A typical example of numerically found stable 1D mixed-mode solitons with  $(N, \gamma, \lambda) = (2, 0, 1)$ . (c) Energies of the 1D semi-dipole and MM solitons versus  $\gamma$  for fixed N = 2 and  $\lambda = 1$ .

#### VII. CONCLUSION

The objective of this work is to construct 2D solitons in the SO (spin-orbit)-coupled two-component BECs, with the contact repulsive interactions whose local strength grows from the center to periphery sufficiently fast. With the anti-Gaussian modulation profile, exact analytical solutions of the SV (semi-vortex) type have been found. These solutions are chiefly controlled by the relative strength of the cross repulsion,  $\gamma$ . The exact solutions exist in the regions of  $\gamma < 1$  and  $\gamma > 2$ . Numerical results demonstrate that exact solutions are stable ground states at  $\gamma < 1$ , while at  $\gamma > 2$  they are unstable excited modes, the ground state being a different solution, found in the numerical form. Other types of 2D solitons, viz, fundamental MMs (mixed modes), and excited state of SVs and MMs are found numerically, as well as the full family of SVs into which the exact analytical solutions are included as particular ones. All the fundamental solutions of both the SV and MM types are completely stable. They are identified as the ground state at  $\gamma > 1$  and  $\gamma < 1$ , respectively, while their excited states, produced by adding vorticity S to both components, are partly stable up to S = 5 and 2, for the SVs and MMs, respectively. The 1D reduction of the system was considered too. In particular, exact states, in the form of semi-dipoles, which are 1D counterparts of the SVs, were found at  $\gamma < 1$ . Families of generic 1D solitons, of the semi-dipole and MM types, have been found in the numerical form. These two types of 1D solitons are close to being mutually degenerate, as they have almost equal

energies.

The present analysis can be further extended. First, a natural possibility is to explore the SO-coupled system with a mixture of Rashba and Dresselhaus coupling terms. Next, one can consider the limit case of strong SO coupling, which makes it possible to neglect the kinetic-energy terms in Eq. (1), thus replacing it by a nonlinear Dirac/Weyl model. Finally, a challenging option is to seek extension of the current setting to the 3D geometry.

#### Acknowledgments

This work was supported, in part, by NNSFC (China) through Grant No. 11575063, 61471123, 61575041, by the joint program in physics between NSF and Binational (US-Israel) Science Foundation through project No. 2015616, by the Israel Science Foundation (project No. 1287/17), and by the Natural Science Foundation of Guangdong Province, through Grant No. 2015A030313639. B.A.M. appreciates a foreign-expert grant of the Guangdong province (China), and a Ding-Ying professorship, provided by the South China Agricultural University (Guangzhou) at its College of Electronic Engineering.

- [1] L. Bergé, Wave collapse in physics: principles and applications to light and plasma waves, Phys. Rep. 303, 259 (1998).
- [2] G. Fibich and G. Papanicolaou, Self-focusing in the perturbed and unperturbed nonlinear Schrödinger equation in critical dimension, SIAM J. Appl. Math. 60, 183 (1999).
- [3] A. S. Desyatnikov, L. Torner, and Y. S. Kivshar, Optical Vortices and Vortex Solitons, Progr. Opt. 47, 1 (2005).
- [4] B. A. Malomed, D. Mihalache, F. Wise, and L. Torner. Spatiotemporal optical solitons. J. Optics B: Quant. Semicl. Opt. 7, R53-R72 (2005); Viewpoint: On multidimensional solitons and their legacy in contemporary Atomic, Molecular and Optical physics, J. Phys. B: At. Mol. Opt. Phys. 49, 170502 (2016).
- [5] D. Mihalache, Multidimensional localized structures in optics and Bose-Einstein condensates: A selection of recent studies, *Rom. Journ. Phys.* **59**, 295-312 (2014).
- [6] B. A. Malomed, Multidimensional solitons: Well-established results and novel findings, Eur. Phys. J. Special Topics 225, 2507 (2016).
- [7] V. S. Bagnato, D. J. Frantzeskakis, P. G. Kevrekidis, B. A. Malomed, and D. Mihalache, Bose-Einstein condensation: Twenty years after, *Rom. Rep. Phys.* **67**, 5 (2015).
- [8] D. Mihalache, Multidimensional localized structures in optical and matter-wave media: A topical survey of recent literature, Rom. Rep. Phys. 69, 403 (2017).
- [9] J. Zeng and B. A. Malomed, Localized dark solitons and vortices in defocusing media with spatially inhomogeneous nonlinearity, Phys. Rev. E **95**, 052214 (2017). X. Gao, J. Zeng, Two-dimensional matter-wave solitons and vortices in competing cubic-quintic nonlinear lattices, *Front. Phys.* **13**, 130501 (2018).
- [10] O. V. Borovkova, Y. V. Kartashov, B. A. Malomed, and L. Torner, Algebraic bright and vortex solitons in defocusing media, Opt. Lett. 36, 3088 (2011).
- [11] O. V. Borovkova, Y. V. Kartashov, L. Torner, and B. A. Malomed, Bright solitons from defocusing nonlinearities, Phys. Rev. E 84, 035602 (R) (2011).
- [12] Y. V. Kartashov, V. A. Vysloukh, L. Torner, and B. A. Malomed, Self-trapping and splitting of bright vector solitons under inhomogeneous defocusing nonlinearities, *Opt. Lett.* **36**, 4587 (2011).
- [13] V. E. Lobanov, O. V. Borovkova, Y. V. Kartashov, B. A. Malomed, and L. Torner, Stable bright and vortex solitons in photonic crystal fibers with inhomogeneous defocusing nonlinearity, Opt. Lett. 37, 1799 (2012).
- [14] Q. Tian, L. Wu, Y. Zhang, and J.-F. Zhang, Vortex solitons in defocusing media with spatially inhomogeneous nonlinearity, Phys. Rev. E 85, 056603 (2012).
- [15] Y. Wu, Q. Xie, H. Zhong, L. Wen, and W. Hai, Algebraic bright and vortex solitons in self-defocusing media with spatially inhomogeneous nonlinearity, *Phys. Rev. A* 87, 055801 (2013).
- [16] R. Driben, Y. V. Kartashov, B. A. Malomed, T. Meier, and L. Torner, Soliton gyroscopes in media with spatially growing repulsive nonlinearity, *Phys. Rev. Lett.* **112**, 020404 (2014).
- [17] Y. V. Kartashov, B. A. Malomed, Y. Shnir, and L. Torner, Twisted toroidal vortex-solitons in inhomogeneous media with repulsive nonlinearity, Phys. Rev. Lett. 113, 264101 (2014).
- [18] R. Driben, Y. Kartashov, B. A. Malomed, T. Meier, and L. Torner, Three-dimensional hybrid vortex solitons, New J. Phys. 16, 063035 (2014).
- [19] J. Hukriede, D. Runde, and D. Kip, Fabrication and application of holographic Bragg gratings in lithium niobate channel waveguides, J. Phys. D 36, R1 (2003).
- [20] G. Roati, M. Zaccanti, C. D'Errico, J. Catani, M. Modugno, A. Simoni, M. Inguscio, and G. Modugno, <sup>39</sup>K Bose-Einstein condensate with tunable interactions, *Phys. Rev. Lett.* **99**, 010403 (2007).
- [21] S. E. Pollack, D. Dries, M. Junker, Y. P. Chen, T. A. Corcovilos, and R. G. Hulet, Extreme tunability of interactions in a 7Li Bose-Einstein condensate, *Phys. Rev. Lett.* **102**, 090402 (2009).

- [22] F. K. Abdullaev, A. Gammal, and L. Tomio, Dynamics of bright matter-wave solitons in a Bose-Einstein condensate with inhomogeneous scattering length, *J. Phys. B: At. Mol. Opt. Phys.* **37**, 635 (2004).
- [23] L. W. Clark, L.-C. Ha, C.-Y. Xu, and C. Chin, Quantum dynamics with spatiotemporal control of interactions in a stable Bose-Einstein condensate, *Phys. Rev. Lett.* **115**, 155301 (2015).
- [24] R. Yamazaki, S. Taie, S. Sugawa, and Y. Takahashi, Quantum dynamics with spatiotemporal control of interactions in a stable Bose-Einstein condensate, Phys. Rev. Lett. 105, 050405 (2010).
- [25] M. Yan, B. J. DeSalvo, B. Ramachandhran, H. Pu, and T. C. Killian, Controlling condensate collapse and expansion with an optical Feshbach resonance, *Phys. Rev. Lett.* 110, 123201 (2013).
- [26] D. M. Bauer, M. Lettner, C. Vo, G. Rempe and S. Dürr, Control of a magnetic Feshbach resonance with laser light, Nature Phys. 5, 339 (2009).
- [27] Y. Li, J. Liu, W. Pang, and B. A. Malomed, Matter-wave solitons supported by field-induced dipole-dipole repulsion with spatially modulated strength, *Phys. Rev. A* 88, 053630 (2013).
- [28] F. Kh. Abdullaev, A. Gammal, B. A. Malomed, and L. Tomio, Bright solitons in Bose-Einstein condensates with field-induced dipole moments, J. Phys. B 47, 075301 (2014).
- [29] Y. Li, Z. Fan, Z. Luo, Y. Liu, H. He, J. Lü, J. Xie, C. Huang, H. Tan, Cross-symmetry breaking of two-component discrete dipolar matter-wave solitons, Front. Phys. 12, 124206 (2017). X. Chen, Y. Chuang, C. Lin, C. Wu, Y. Li, B. A. Malomed, and R. Lee, Magic tilt angle for stabilizing two-dimensional solitons by dipole-dipole interactions, Phys. Rev. A 96, 043631 (2017). Y. Li, W. Pang, J. Xu, C. Lee, B. A. Malomed, L. Santos, Long-range transverse Ising model built with dipolar condensates in two-well arrays, New. J. Phys. 19, 013030 (2017)
- [30] Y. J. Lin, K. Jimenez-Garcia, and I. B. Spielman, Spin-orbit-coupled Bose-Einstein condensates, Nature 471, 83 (2011).
- [31] D. L. Campbell, G. Juzeliūnas, and I. B. Spielman, Realistic Rashba and Dresselhaus spin-orbit coupling for neutral atoms, Phys. Rev. A 84, 025602 (2011).
- [32] Y. Zhang, L. Mao, and C. Zhang, Mean-field dynamics of spin-orbit coupled Bose-Einstein condensates, Phys. Rev. Lett. 108, 035302 (2012).
- [33] V. Galitski and I. B. Spielman, Spin-orbit coupling in quantum gases, Nature 494, 49-54 (2013).
- [34] H. Zhai, Degenerate quantum gases with spin-orbit coupling: a review, Rep. Prog. Phys. 78 026001(2015).
- [35] Z. Wu, L. Zhang, W. Sun, X.-T. Xu, B.-Z. Wang, S.-C. Ji, Y. Deng, S. Chen, X.-J. Liu, and J.-W. Pan, Realization of two-dimensional spin-orbit coupling for Bose-Einstein condensates, Science 354, 83 (2016).
- [36] Z. Meng, L. Huang, P. Peng, D. Li, L. Chen, Y. Xu, C. Zhang, P. Wang, and J. Zhang, Experimental Observation of a Topological Band Gap Opening in Ultracold Fermi Gases with Two-Dimensional Spin-Orbit Coupling, *Phys. Rev. Lett.* 117, 235304 (2016).
- [37] Y. Zhang, M. E. Mossman, T. Busch, P. Engels, C. Zhang, Properties of spin-orbit-coupled Bose-Einstein condensates, Front. Phys. 11, 118103 (2016).
- [38] C. Wang, C. Gao, C.-M. Jian, and H. Zhai, Spin-orbit coupled spinor Bose-Einstein condensates, *Phys. Rev. Lett.* **105**, 160403 (2010).
- [39] T. Kawakami, T. Mizushima, and K. Machida, Textures of F=2 spinor Bose-Einstein condensates with spin-orbit coupling, *Phys. Rev. A* 84, 011607 (2011).
- [40] B. Ramachandhran, B. Opanchuk, X.-J. Liu, H. Pu, P. D. Drummond, and H. Hu, Half-quantum vortex state in a spin-orbit-coupled Bose-Einstein condensate, Phys. Rev. A 85, 023606 (2012).
- [41] G. J. Conduit, Line of Dirac monopoles embedded in a Bose-Einstein condensate, Phys. Rev. A 86, 021605(R) (2012).
- [42] T. Kawakami, T. Mizushima, M. Nitta, and K. Machida, Stable skyrmions in SU(2) gauged Bose-Einstein condensates, Phys. Rev. Lett. 109, 015301 (2012).
- [43] V. Achilleos, D. J. Frantzeskakis, P. G. Kevrekidis, and D. E. Pelinovsky, Matter-Wave Bright Solitons in Spin-Orbit Coupled Bose-Einstein Condensates, *Phys. Rev. Lett.* **110**, 264101 (2013).
- [44] Y. V. Kartashov, V. V. Konotop, and F. Kh. Abdullaev, Gap Solitons in a Spin-Orbit-Coupled Bose-Einstein Condensate, Phys. Rev. Lett. 111, 060402 (2013).
- [45] Y. Xu, Y. Zhang, and B. Wu, Bright solitons in spin-orbit-coupled Bose-Einstein condensates, Phys. Rev. A 87, 013614 (2013).
- [46] H. Sakaguchi and B. Li, Vortex lattice solutions to the Gross-Pitaevskii equation with spin-orbit coupling in optical lattices, Phys. Rev. A 87, 015602 (2013).
- [47] D. A. Zezyulin, R. Driben, V. V. Konotop, and B. A. Malomed, Nonlinear modes in binary bosonic condensates with pseudo-spin-orbital coupling, *Phys. Rev. A* 88, 013607 (2013).
- [48] L. Salasnich and B.A. Malomed, Localized modes in dense Bose-Einstein condensates with spin-orbit and Rabi couplings, Phys. Rev. A 87, 063625 (2013).
- [49] Y. Cheng, G. Tang, and S. K. Adhikari, Localization of a spin-orbit-coupled Bose-Einstein condensate in a bichromatic optical lattice, *Phys. Rev. A* 89, 063602 (2014).
- [50] L. Salasnich, W. B. Cardoso, and B. A. Malomed, Localized modes in quasi-two-dimensional Bose-Einstein condensates with spin-orbit and Rabi couplings, Phys. Rev. A 90, 033629 (2014).
- [51] V. E. Lobanov, Y. V. Kartashov, and V. V. Konotop, Fundamental, multipole, and halfvortex gap solitons in spin-orbit coupled Bose-Einstein condensates, *Phys. Rev. Lett.* 112, 180403 (2014).
- [52] H. Sakaguchi and B. A. Malomed, Discrete and continuum composite solitons in Bose- Einstein condensates with the Rashba spin-orbit coupling in one and two dimensions, *Phys. Rev. E* **90**, 062922 (2014).
- [53] S. Gautam and S. K. Adhikari, Vector solitons in a spin-orbit-coupled spin-2 Bose-Einstein condensate, Phys. Rev A 91, 063617 (2015).

- [54] Y. Zhang, Y. Xu, and T. Busch, Gap solitons in spin-orbit-coupled Bose-Einstein condensates in optical lattices, Phys. Rev. A 91, 043629 (2015).
- [55] X. Zhu, H. Li and Z. Shi, Defect matter-wave gap solitons in spin-orbit-coupled Bose-Einstein condensates in Zeeman lattices, *Phys. Lett. A* **380**, 3253 (2016). H. Lia, X. Zhua, Z. Shi, Inverted solitons in a spin-orbit-coupled Bose-Einstein condensate, *Opt. Comm.* **392** 214 (2017).
- [56] L. Wen, Q. Sun, Y. Chen, D.-S. Wang, J. Hu, H. Chen, W.-M. Liu, G. Juzeliūnas, B. A. Malomed, and A.-C. Ji, Motion of solitons in one-dimensional spin-orbit-coupled Bose-Einstein condensates, *Phys. Rev. A* 94, 061602(R) (2016).
- [57] Y. Li, J. Xue, Stationary and moving solitons in spin "Corbit-coupled spin-1 Bose" CEinstein condensates, Front. Phys. 13, 130307 (2018).
- [58] G. Gligorić, A. Maluckov, Lj. Hadzievski, S. Flach, and B. A. Malomed, Nonlinear localized flatband modes with spin-orbit coupling, *Phys. Rev. B* **94**, 144302 (2016).
- [59] Y. V. Kartashov and V. V. Konotop, Solitons in Bose-Einstein condensates with helicoidal spin-orbit coupling, Phys. Rev. Lett. 118, 190401 (2017).
- [60] Y. Li, Y. Liu, Z. Fan, W. Pang, S. Fu, and B. A. Malomed, Two-dimensional dipolar gap solitons in free space with spin-orbit coupling, Phys. Rev. A 95, 063613 (2017).
- [61] H. Sakaguchi, and B. A. Malomed, One- and two-dimensional gap solitons in spin-orbit-coupled systems with Zeeman splitting, Phys. Rev. A 97, 013607 (2018).
- [62] J. Dias, M. Figueira, V. V. Konotop, Coupled nonlinear Schrödinger equations with a gauge potential: Existence and blowup, Stud. Appl. Mat. 136, 241 (2015).
- [63] Sh. Mardonov, E. Ya. Sherman, J. Muga, H. W. Wang, Y. Ban, and X. Chen, Collapse of spin-orbit-coupled Bose-Einstein condensates, Phys. Rev. A 91, 043604 (2015).
- [64] H. Sakaguchi, B. Li, and B. A. Malomed, Creation of two-dimensional composite solitons in spin-orbit-coupled selfattractive Bose-Einstein condensates in free space, Phys. Rev. E 89, 032920 (2014).
- [65] H. Sakaguchi, E. Ya. Sherman, and B. A. Malomed, Vortex solitons in two-dimensional spin-orbit coupled Bose-Einstein condensates: Effects of the Rashba-Dresselhaus coupling and the Zeeman splitting, *Phys. Rev. E* **94**, 032202 (2016).
- [66] G. Chen, Y. Liu, and H. Wang, Mixed-mode solitons in quadrupolar BECs with spin-orbit coupling, Commun. Nonlinear Sci. Numer. Simulat. 48, 318 (2017).
- [67] Y. V. Kartashov, B.A. Malomed, V. V. Konotop, V. E. Lobanov, and L. Torner, Stabilization of solitons in bulk Kerr media by dispersive coupling, Opt. Lett. 40, 1045 (2015).
- [68] C.-E. Bardyn, T. Karzig, G. Refael, and T. C. H. Liew, Phys. Rev. B 91, 161413 (2015).
- [69] A. V. Nalitov, D. D. Solnyshkov, and G. Malpuech, Phys. Rev. Lett. 114, 116401 (2015).
- [70] Y. V. Kartashov and D. V. Skryabin, Two-dimensional lattice solitons in polariton condensates with spin-orbit coupling, Opt. Lett. 41, 5043 (2016).
- [71] H. Sakaguchi, B. A. Malomed, and D. V. Skryabin, Spin-orbit coupling and nonlinear modes of the polariton condensate in a harmonic trap. New J. Phys. 19, 08503 (2017).
- [72] Y.-C. Zhang, Z.-W. Zhou, B. A. Malomed, and H. Pu, Stable solitons in three dimensional free space without the ground state: Self-trapped Bose-Einstein condensates with spin-orbit coupling, *Phys. Rev. Lett.* **115**, 253902 (2015).
- [73] Y. Xu, Y. Zhang, and C. Zhang, Bright solitons in a 2D spin-orbit-coupled dipolar Bose-Einstein condensate, Phys. Rev. A 92, 013633 (2015).
- [74] X. Jiang, Z. Fan, Z. Chen, W. Pang, Y. Li, and B. A. Malomed, Two-dimensional solitons in dipolar Bose-Einstein condensates with spin-orbit coupling, *Phys. Rev. A* **93**, 023633 (2016).
- [75] B. Liao, S. Li, F. Wang, C. Huang, Z. Luo, W. Pang, H. Tan, B. A. Malomed, Y. Li, Anisotropic semi-vortices in dipolar Bose-Einstein condensates controlled by the Zeeman-splitting potential, *Phys. Rev. A* **96**, 043613 (2017).
- [76] Y. A. Bychkov and E. I. Rashba, Oscillatory effects and the magnetic susceptibility of carriers in inversion layers, J. Phys. C 17, 6039 (1984).
- [77] E. I. Rashba and E. Y. Sherman, Spin orbital band splitting in symmetric quantum wells, Phys. Lett. A 129, 175-179 (1988).
- [78] H. Sakaguchi and B. A. Malomed. Solitons in combined linear and nonlinear lattice potentials, Phys. Rev. A 81, 013624 (2010).
- [79] D. Kaup, B. Malomed, Soliton trapping and daughter waves in the Manakov model, Phys. Rev. A 48, 599 (1993).
- [80] Y. Li, Z. Luo, Y. Liu, Z. Chen, C. Huang, S. Fu, H. Tan, and B. A. Malomed, Two-dimensional solitons and quantum droplets supported by competing self- and cross-interactions in spin-orbit-coupled condensates, New J. Phys. 19 113043 (2017).
- [81] C. Huang, H. He, W. Pang, B. A. Malomed, Y. Li, Excited state of two-dimensional matter-wave solitons supported by field-induced dipole-dipole repulsion and spin-orbit coupling, *Phys. Rev. A* 97, 013636 (2018).
- [82] A. C. White, Y. Zhang, and T. Busch, Odd-petal-number states and persistent flows in spin-orbit-coupled Bose-Einstein condensates, *Phys. Rev. A* **95**, 041604(R) (2017). X. Zhang, M. Kato, W. Han, S. Zhang, and H. Saito, Spin-orbit-coupled Bose-Einstein condensates held under a toroidal trap, *Phys. Rev. A* **95**, 033620 (2017).